Complement 3a Receptor 1 on Macrophages and Kupffer cells is not required for the Pathogenesis of Metabolic Dysfunction-Associated Steatotic Liver Disease

Edwin A. Homan[1], Ankit Gilani[1], Alfonso Rubio-Navarro[1], Maya A. Johnson[1], Odin M. Schaepkens[1], Eric Cortada[1], Renan Pereira de Lima[1], Lisa Stoll[1], James C. Lo[1*].

Affiliations:

[1] Division of Cardiology, Department of Medicine, Cardiovascular Research Institute, Weill Center for Metabolic Health, Weill Cornell Medicine, New York, New York, 10021

*Corresponding author. Email: jlo@med.cornell.edu.

Abstract

Together with obesity and type 2 diabetes, metabolic dysfunction-associated steatotic liver disease (MASLD) is a growing global epidemic. Activation of the complement system and infiltration of macrophages has been linked to progression of metabolic liver disease. The role of complement receptors in macrophage activation and recruitment in MASLD remains poorly understood. In human and mouse, *C3AR1* in the liver is expressed primarily in Kupffer cells, but is downregulated in humans with MASLD compared to obese controls. To test the role of complement 3a receptor (C3aR1) on macrophages and liver resident macrophages in MASLD, we generated mice deficient in C3aR1 on all macrophages (C3aR1-MφKO) or specifically in liver Kupffer cells (C3aR1-KpKO) and subjected them to a model of metabolic steatotic liver disease. We show that macrophages account for the vast majority of *C3ar1* expression in the liver. Overall, C3aR1-MφKO and C3aR1-KpKO mice have similar body weight gain without significant alterations in glucose homeostasis, hepatic steatosis and fibrosis, compared to controls on a MASLD-inducing diet. This study demonstrates that C3aR1 deletion in macrophages or Kupffer cells, the predominant liver cell type expressing *C3aR1*, has no significant effect on liver steatosis, inflammation or fibrosis in a dietary MASLD model.

Keywords: obesity, hepatic steatosis, steatohepatitis, C3aR1, macrophage, Kupffer cell

Introduction

Obesity and related metabolic diseases such as type 2 diabetes (T2D) and metabolic dysfunction-associated steatotic liver disease (MASLD) remain a worldwide epidemic with increasing prevalence[1,2]. MASLD describes the constellation of hepatic lipid deposition, inflammation, and fibrosis associated with obesity and T2D that ultimately leads to MASH cirrhosis, which has become the leading cause of liver transplantation in the United States[3-6]. Notably, MASLD is increasingly recognized as an important risk-enhancing factor for atherosclerotic cardiovascular disease[7,8].

Liver macrophages help to maintain hepatic homeostasis and consist of embryo-derived resident macrophages called Kupffer cells, which self-renew and do not migrate, or peripheral monocyte-derived macrophages, which infiltrate into liver tissue upon metabolic or toxic liver injury and under certain circumstances can take on Kupffer cell-like identity[9-13]. In obesity, bone marrow-derived myeloid cells migrate to the steatotic liver, and pro-inflammatory recruited macrophages are postulated to drive the progression of MASLD to MASH[14]. Spatial proteogenomics reveals a population of lipid-associated macrophages near bile canaliculi that is induced by local lipid exposure and drives fibrosis in steatotic regions of murine and human liver[15]. In addition, deep transcriptomic profiling in human MASLD has identified candidate gene signatures for steatohepatitis and fibrosis with possible therapeutic implications[16].

Activation of the body's complement system leads to increased cell lysis, phagocytosis, and inflammation[17], and it is increasingly recognized as an important contributor to regulation of metabolic disorders such as T2D and MASLD[18,19]. In human liver biopsies, higher lobular inflammation scores correlate with activation of the complement alternative pathway[20], which can signal *via* the C3a receptor 1 (C3aR1), a G_i-coupled G protein-coupled receptor[21]. The complement 3 polypeptide (C3) is cleaved by C3 convertase to the activated fragment, C3a, which then binds C3aR1[22]. Complement factor D (CFD), also known as the adipokine adipsin, is the rate-limiting step in the alternative pathway of complement activation[23,24].

59 Several studies have reported opposing roles of adipsin and C3aR1 on hepatic steatosis
60 in diet-induced obesity[25-27]. Our lab has found that adipsin/CFD is critical for maintaining
61 pancreatic beta cell mass and function[28,29]. Murine obese and diabetic models such as *db/db*
62 mice and high fat diet (HFD) feeding result in very low circulating adipsin[23]. Replenishing adipsin
63 in *db/db* mice raises levels of C3a and insulin, lowers blood glucose levels, and inhibits hepatic
64 gluconeogenesis[28]. However, whole-body deletion of C3aR1 decreases macrophage infiltration
65 and activation in adipose tissue, protects from HFD-induced obesity and glucose intolerance,
66 and decreases hepatic steatosis and inflammation[30]. In a model of fibrosing steatohepatitis,
67 bone marrow-derived macrophages were found to activate hepatic stellate cells, which was
68 blunted in whole-body C3aR1 KO mice[31].
69 In the present study we aim to explore the macrophage-specific effect of complement
70 receptor signaling in MASLD pathogenesis. To determine the consequences of macrophage and
71 Kupffer cell ablation of C3aR1, we use a murine dietary model of MALFD/MASH, the Gubra
72 Amylin Nash (GAN) diet, which has macronutrient similarities to the Western diet and produces
73 similar histologic and transcriptomic changes to human MASLD/MASH[32-34].
74
75 **Results**
76 *C3AR1 is expressed in human and mouse liver, primarily in Kupffer cells.*
77 In the scRNA-Seq database, Human Protein Atlas, *C3AR1* is broadly expressed
78 throughout the body, with increased abundance in tissues rich in immunologic cell types, such
79 as bone marrow and appendix (Fig. 1A)[35]. In a single-cell transcriptomic database of healthy
80 human liver, *C3AR1* expression predominates in the macrophage and Kupffer cell population,
81 with minimal-to-undetectable *C3AR1* expression in hepatocytes or hepatic stellate cells by
82 scRNA-Seq (Fig. 1B)[36]. In the mouse liver scRNA-Seq database, Tabula Muris, *C3ar1* is
83 similarly expressed primarily in Kupffer cells (Fig. S1)[37].
84

85 *Hepatic CFD and C3AR1 are downregulated in human MASLD/MASH.*

86 We also examined data from Suppli and coworkers, who performed bulk transcriptomic
87 analysis of human liver samples from an age-matched cohort of healthy controls and obese
88 controls without MASLD, as well as MASLD and MASH patients without cirrhosis[38]. Both *CFD*
89 *and C3AR1* were unchanged in obese subjects without MASLD compared to healthy controls,
90 but both *CFD* and *C3AR1* were significantly downregulated in liver biopsies from both MASLD
91 and MASH patients compared to both healthy controls and obese subjects without MASLD (Fig.
92 1C). Interestingly, both *CFD* and *C3AR1* levels were slightly higher in MASH individuals
93 compared to those with MASLD only.

94 *Murine MASH model recapitulates key features of human MASH*

95 At 5 weeks of age, we subjected *C3ar1* flox/flox control mice to standard regular diet
96 (RD) or GAN diet[32,33]. After 28 weeks of GAN diet, male mice gained body weight compared to
97 RD (Fig. 1D), primarily as fat mass (Fig. S2-3), but weight gain in female GAN-fed mice was
98 attenuated. Histologic signs of MASLD were present in GAN-fed mice (Fig. 1E), most notably
99 hepatic steatosis and hepatocyte ballooning (Fig. 1F), and liver fibrosis measured by collagen
100 deposition nearly doubled with GAN compared to RD (Fig. 1G). Both hepatic *C3ar1* and *Cfd*
101 gene expression were robustly increased on GAN compared to RD, as were markers of
102 macrophage infiltration, hepatic inflammation, and fibrosis, including collagen gene expression,
103 indicating progression to fibrotic MASH (Fig. 1H). In female control mice on GAN diet, there
104 were no significant differences in *C3ar1* expression or other gene markers, though there was a
105 nonsignificant trend toward increased inflammation and fibrosis compared to regular diet (Fig.
106 S4).

107 *Macrophage-specific C3aR1 deletion does not alter glucose homeostasis.*

108 Owing to higher levels of *C3ar1* in murine MASLD and the differential regulation of
109 *C3AR1* gene in MASLD humans, this motivated us to interrogate the role of pathophysiological
110 role of *C3ar1* in macrophages in MASLD. We generated transgenic mice with macrophage-

111 specific deletion of C3aR1 by crossing *C3ar1* floxed mice with LysM-Cre transgenic mice
112 (C3aR1-MφKO) to target both liver resident macrophages and recruited monocytes. *C3ar1*
113 floxed mice were used as controls. Successful deletion of *C3ar1* in macrophages from the
114 C3aR1-MφKO mouse was confirmed by quantitative RT-PCR of isolated peritoneal
115 macrophages that were F4/80+ and CD68+ by fluorescence-activated cell sorting (Fig. 2A). In
116 liver tissue, *C3ar1* expression was reduced by ~88% in both male and female C3aR1-MφKO
117 (Fig. 2B). These results indicate that macrophages account for the vast majority of *C3ar1*
118 expression in the liver.

119 When placed on GAN diet, there was no significant difference in weight gain between
120 control and C3aR1-MφKO mice (Fig. 2C). There was similarly no difference in percent lean or
121 fat mass between these mice (Fig. 2D). Glucose tolerance tests performed in fasted mice after
122 27 weeks GAN diet found no significant differences between control and C3aR1-MφKO mice
123 (Fig. 2E). There was also no difference in insulin sensitivity as measured by insulin tolerance
124 tests in male mice (Fig. S5). Insulin resistance as measured by comparing the ratio of fasting
125 glucose level to fasting insulin level (HOMA-IR) was also unchanged between controls and
126 C3aR1-MφKO mice (Fig. S6). Circulating serum ALT levels were unchanged in male control and
127 C3aR1-MφKO mice on GAN diet (Fig. S7).

128 *Macrophage-specific C3aR1 deletion does not significantly impact hepatic steatosis or fibrosis.*

129 Liver samples collected after 28-30 weeks of GAN or regular diet did not show significant
130 differences in liver mass between control and C3aR1-MφKO mice (Fig. 2F). Male mice on GAN
131 diet developed similar qualitative appearance on histology (Fig. 2G), and slide image analysis
132 showed similar proportions of lipid droplet area and collagen area (Figs. 2H, 2I). This indicates
133 that there were no significant differences in steatosis or fibrosis between GAN-fed control and
134 C3aR1-MφKO male mice. While *C3ar1* expression was markedly reduced in the C3aR1-MφKO
135 liver tissue (Fig. 2B), there were no detectable gene expression changes in markers of fibrosis,

136 inflammation, or lipid handling on either GAN or regular diet (Fig. 2J-K). Similarly, in female mice
137 there were also no significant differences between control and C3aR1-MφKO mouse liver on
138 either GAN or regular diet in a subset of key gene markers of fibrosis or inflammation (Fig. S8).
139
140 *Kupffer cell-specific C3aR1 deletion does not alter weight gain or glucose homeostasis.*
141 To explore whether there may be competing effects between recruited monocytes and
142 liver resident macrophages (Kupffer cells), we next generated Kupffer cell-specific C3aR1
143 knockout mice (C3aR1-KpKO) by crossing *C3ar1* floxed mice to Clec4f-Cre transgenic mice and
144 fed them GAN diet. *C3ar1* floxed mice were used as controls. Body weight gain was similar
145 between genotypes for both male and female mice (Fig. 3A), and there was no difference in
146 body composition between control and C3aR1-KpKO mice on GAN diet (Fig. 3B). There was
147 similarly no significant difference in glucose homeostasis between the genotypes during a
148 glucose tolerance test (Fig. 3C).
149 *Kupffer cell-specific C3aR1 deletion does not significantly impact hepatic steatosis or fibrosis.*
150 Liver mass was not significantly different between control and C3aR1-KpKO mice on
151 GAN diet (Fig. 3D). Liver sections appeared qualitatively similar by histology stained with
152 Masson's trichrome (Fig. 3E). There were similar levels of hepatic steatosis in these mice as
153 measured by percent lipid droplet area (Fig. 3F). When measured by collagen proportional area,
154 there was no significant differences in liver fibrosis between C3aR1-KpKO and control mice
155 (Fig. 3G). While *C3ar1* expression was reduced by 73% in liver tissue of C3aR1-KpKO mice,
156 there were no significant differences in expression of inflammatory, fibrotic, or lipid handling
157 gene markers (Fig. 3H). *C3ar1* expression similarly decreased by ~90% in liver tissue of female
158 C3aR1-KpKO mice fed regular diet compared to control mice (Fig. S9). These data also indicate
159 that Kupffer cells account for ~80% of hepatic *C3ar1* gene expression in our mouse model of
160 MASLD/MASH.
161 **Discussion**

162 Overall, we found that macrophage or Kupffer cell expression of *C3ar1* does not impact
163 body weight gain or histologic/transcriptomic features of MASLD/MASH in a murine dietary
164 model. Deletion of C3aR1 in the macrophage population throughout the body, or specifically in
165 Kupffer cells, did not affect weight gain, glucose homeostasis, or extent of hepatic
166 steatosis/fibrosis. With long term GAN diet feeding that has been previously shown to model
167 human MASLD/MASH, we did not observe significant differences in liver abnormalities with the
168 KO mice.

169 Our findings in macrophage-specific C3aR1 KO mice contrast with prior observations in
170 whole-body C3aR1 KO mice[30], which are protected from diet-induced obesity, have improved
171 glucose tolerance, and exhibit decreased hepatic steatosis. In both our macrophage- and
172 Kupffer cell-specific C3aR1 KO mice, which had similar degrees of obesity compared to
173 controls, there was no detectable effect on liver steatosis or fibrosis despite the near abrogation
174 of *C3ar1* expression. This raises the possibility that the lower levels of hepatic steatosis and
175 insulin resistance previously observed in the whole body C3aR1 KO mice may be secondary to
176 protection from obesity. Protection from diet-induced obesity in whole-body C3aR1 KO mice
177 may be mediated by a non-macrophage cell type, since our macrophage-specific C3aR1 KO
178 mice were not afforded this protection. The *C3ar1*-expressing cell types that promote obesity
179 and MASLD remains to be determined.

180 Our laboratory recently reported sex-dependent regulation of thermogenic adipose
181 tissue mediated by adipocyte-derived C3aR1[39]. However, no such sexual dimorphism was
182 observed in hepatic expression of key MASH genes in response to GAN diet in our
183 macrophage- or Kupffer cell-specific C3aR1-deficient mice. Other work has suggested possible
184 compensatory effects from its sister anaphylatoxin receptor C5aR1, with increased cold-induced
185 adipocyte browning and attenuated diet-induced obesity seen in C3aR1/C5aR1 double KO
186 mice[40].

The strengths of our study include careful metabolic and transcriptomic phenotyping of cell type-specific transgenic mice. Some limitations were our use of a single MASLD dietary model and our focus on the C3aR1 pathway. While the GAN diet recapitulates many features of human MASH due to its similarity to Western diet[34], relatively low levels of fibrosis were seen in our study, potentially related to initiating the diet at young age; more rapid fibrosis induction has been seen when GAN diet is initiated at older ages[41]. It is possible that in other models of liver injury that we did not test (e.g., short-term treatment with a hepatotoxin such as carbon tetrachloride),[42] there may be differences in liver injury in mice lacking *C3ar1* in macrophages. However, the GAN diet model has been shown to better parallel the gene expression changes in human MAFLD/MASH.[33] Lastly, while *C3AR1*/*C3ar1* expression is very low in non-macrophage cells (Fig. B, S1), C3aR1 signaling on other hepatic cell types not explored in this study, such as hepatic stellate cells, could mediate the observed effect in the whole-body C3aR1 KO mouse.

Deletion of C3aR1 in macrophages generally, or in liver resident macrophages specifically, had no major effect on systemic glucose homeostasis and hepatic steatosis, inflammation, and fibrosis in this murine dietary model of MASLD/MASH. The complement system is a complex entity directing an important part of the body's inflammatory and tissue repair response in MASLD. Further work is needed to elucidate the mechanisms of the role of C3aR1 in the pathogenesis of MASH and cirrhosis.

208 **Materials and Methods**

209 *Animals*

210 *C3ar1 flox/flox* mice were on the C57BL/6J background as described[43]. Homozygous
211 LysM-Cre mice on the C57BL/6J background (Strain #004781) as well as homozygous Clec4f-
212 Cre mice on the C57BL/6J background (Strain #003296) were purchased from Jackson
213 Laboratories. *C3ar1 flox/flox* homozygous mice on C57BL/6J background were used in the
214 experiments as controls from the same backcross generation[39]. All mice were maintained in
215 plastic cages under a 12h/12h light/dark cycle at constant temperature (22°C) with free access
216 to water and food. Mice were fed regular diet containing 4.5%kcal fat PicoLab Rodent diet 20
217 (LabDiet) or GAN diet containing 40%kcal HFD (mostly palm oil) with 20% fructose and 2%
218 cholesterol (D09100310, Research Diets) for 28-30 weeks. Fat mass and lean mass were
219 determined via noninvasive 3-in-1 body composition analyzer (EchoMRI). Mice were humanely
220 euthanized with CO_2 inhalation followed by exsanguination by cardiac puncture.

221 *Blood chemistry and serum insulin analysis*

222 Mice were fasted overnight (14-16 hours) for glucose tolerance tests and injected
223 intraperitoneally with syringe-filtered D-glucose solution (2g/kg). For insulin tolerance test, mice
224 were fasted for 6 hours and injected with 0.5 mIU/kg insulin. Blood glucose levels were assayed
225 by commercial glucometer (OneTouch) by tail vein blood samples. Plasma insulin levels were
226 measured from mice fasted for 6 hours. Tail vein blood was collected into lithium heparin-coated
227 tubes, centrifuged at 2000xg at 4ºC, and plasma insulin levels were determined by ELISA using
228 a standard curve (Mercodia). Serum alanine aminotransferase levels were measured in serum
229 from blood collected via cardiac puncture using a commercially available colorimetric assay
230 (TR71121, ThermoFisher Scientific).

231 *Peritoneal macrophage isolation and flow cytometry*

232 Peritoneal macrophages were isolated from as previously described[44]. Briefly, mice
233 were euthanized then immediately injected intraperitoneally with 10 mL phosphate-buffered

234 saline (PBS, pH 7.4) at room temperature. After a 3-5 minute incubation period, peritoneal fluid
235 was removed with sterile needle and syringe and placed on ice. After centrifugation at 300xg,
236 the pellet was resuspended in PBS containing 2% fetal bovine serum and 0.1% sodium azide.
237 Cells were stained with phycoerythrin-conjugated anti-F4/80 (clone BM8, cat. #123110) and
238 fluorescein isothiocyanate-conjugated anti-CD11b (clone M1/70, cat. #101206) fluorescent
239 antibodies (Biolegend). Stained cells were loaded on MA900 fluorescence-activated cell sorter
240 (Sony), and dual-positive F480+/CD11b+ cells were sorted for subsequent RNA extraction.

241 *Histological studies*

242 A mid-distal portion of the left liver lobe was fixed with 10% buffered formalin and
243 transferred to 70% ethanol. Samples were embedded in paraffin, sectioned at ~5μm thickness,
244 and stained with Masson's trichrome. Slides were imaged using Zeiss Axioscan7 at 20x
245 magnification. Histologic analyses were performed using ImageJ software (version 1.53t). Lipid
246 droplet area was quantified by subtracting non-droplet area in the green channel from total
247 section area of 2-3 independent sections. Collagen proportionate area was quantified by
248 measuring total area in the red channel after reducing intensity threshold to 60-70.

249 *RNA extraction and real-time quantitative PCR analysis*

250 Total RNA from liver tissue lysates was extracted using Trizol reagent (Invitrogen)
251 followed by RNAeasy Mini kit (Qiagen) as per manufacturer's protocol. RNA was reverse-
252 transcribed using the High Capacity cDNA RT kit (Thermo). Quantitative PCR was performed
253 using SYBR Green Master Mix (Quanta) and specific gene primers on QuantStudio6 Flex Real-
254 Time PCR Systems (Thermo Fisher Scientific) using the delta-delta Ct method. Expression
255 levels were normalized to Ribosomal protein S18 (*Rps18*). Primer sequences are listed in
256 Supplementary Table A.

257 *Statistical analyses*

258 All statistical analyses were performed using GraphPad Prism10. Unpaired two-tailed

Student's *t* test with Welch correction for most analyses, with Holm-Šídák correction for multiple comparisons where applicable, and $p<0.05$ was considered statistically significant.

Funding

E.A.H. was supported by NIH T32 5T32HL160520-02. A.G. was supported by ADA 9-22-PDFPM-01. R.P.L was supported by AHA 23DIVSUP1074485. L.S. was supported by AHA 908952 and an Ehrenkranz Young Scientist Award. J.C.L. was supported by NIH R01 DK121140, R01 DK121844, and R01 DK132879. The views expressed in this manuscript are those of the authors and do not necessarily represent the official views of the American Diabetes Association, the American Heart Association, the National Institute of Diabetes and Digestive and Kidney Diseases, or the National Institutes of Health.

Acknowledgments

We would like to thank Dr. Baran Ersoy, Dr. Robert Schwartz, and Dr. Saloni Sinha for their technical advice and assistance.

Declaration of Competing Interest

None

Data Availability

Data will be made available upon reasonable request.

276 **Figure Legends**

277

278 **Figure 1. C3AR1 is found in macrophages, is modulated by MASLD/MASH in humans,**
279 **and is induced by a murine dietary model of MASH.**

280 A) Relative *C3AR1* human tissue expression level by tissue, derived from deep sequencing
281 of the mRNA combined dataset (HPA and GTEx) in the Human Protein Atlas, shown as
282 normalized transcripts per million (nTPM). Liver is highlighted in purple and immunologic
283 tissues are highlighted in red.

284 B) Single-cell RNA sequencing distribution of *C3AR1* expression in human liver (tSNE, t-
285 distributed Stochastic Neighbor Embedding).

286 C) Analysis of *CFD* and *C3AR1* expression from liver biopsy samples in patients with
287 MASH, MASLD, obesity without MASLD, and age-matched healthy controls (n = 12-16
288 per group, Welch *t* test with Holm-Šídák correction for multiple comparisons).

289 D) Weight curve in male and female flox/flox control mice placed on GAN high-fat diet
290 compared to regular diet (RD) controls (males, n = 7; females, n = 6).

291 E) Representative liver section staining by Masson's Trichrome in male control mice on RD
292 or GAN diet for 28 weeks (scale bar = 100 mm).

293 F) Lipid droplet area quantification in liver sections from male control mice, excluding
294 vessel lumens (RD, n = 3; GAN, n = 7).

295 G) Collagen area quantification in liver sections of male control mice (RD, n = 3; GAN, n =
296 7).

297 H) Gene expression of key macrophage or fibrosis genes in male control mice on GAN or
298 RD (n = 6 per group).

299 Unpaired two-tailed Student's *t* test (Except 1C as above). Annotations: *, $p < 0.05$; **, $p < 0.01$;
300 ***, $p < 0.001$

301 **Figure 2. C3aR1 deletion in all macrophages does not affect weight gain, glucose**
302 **homeostasis, liver steatosis or fibrosis.**

303 A) Expression of *C3ar1* in isolated peritoneal F4/80+/CD68+ cells from flox/flox control mice
304 (n = 6) or C3aR1-MφKO male mice (n = 3).

305 B) Expression of *C3ar1* in whole liver from control or C3aR1-MφKO mice (n = 11-12 per
306 male group, n = 13-14 per female group).

307 C) Body mass curve of control or C3aR1-MφKO mice on GAN high-fat diet starting at 5
308 weeks of age (n = 11-12 per male group, n = 14 per female group).

309 D) Body composition analysis by EchoMRI in control or C3aR1-MφKO mice after 30 weeks
310 GAN diet (n = 6-9 per male group, n = 9-13 per female group).

311 E) Glucose tolerance test in control or C3aR1-MφKO mice with 14h fast after 28 weeks
312 GAN diet (n = 6-9 per male group, n = 9-14 per female group).

313 F) Liver mass in control or C3ar1-MφKO male mice at time of euthanasia after 30 weeks
314 GAN diet (n = 6-9 per male group, n = 9-14 per female group).

315 G) Representative liver section staining by Masson's Trichrome in male control or C3ar1-
316 MφKO mice (scale bar = 100 mm).

317 H) Lipid droplet area in liver sections from male control or C3ar1-MφKO mice, excluding
318 vessel lumens (n = 6-7 per group).

319 I) Collagen area in liver sections from male control or C3ar1-MφKO mice (n = 6-7 per
320 group).

321 J,K) Relative mRNA expression of key markers for inflammation, fibrosis, and liver
322 metabolism in liver from male control or C3ar1-MφKO mice after 30 weeks of either GAN (J)
323 diet (n = 11-12 per group) or regular (K) diet (n = 3-5 per group).

324 Unpaired two-tailed Student's *t* test: Student's *t* test: *, $p < 0.05$.

325

326 **Figure 3. C3aR1 deletion in Kupffer cells does not affect weight gain, glucose**
327 **homeostasis, liver steatosis or fibrosis.**

328 A) Body mass curve on GAN diet in flox/flox control or C3aR1-KpKO mice beginning at 5
329 weeks of age (n = 8-10 per group).
330 B) Body composition analysis by EchoMRI in control or C3aR1-KpKO mice after 28 weeks
331 GAN diet (n = 8-10).
332 C) Glucose tolerance test in control or C3aR1-KpKO mice with 14h fast after 26 weeks
333 GAN diet (n = 8-10).
334 D) Liver mass in control or C3aR1-KpKO male mice at time of euthanasia after 30 weeks
335 GAN diet (n = 8-10).
336 E) Representative liver section staining by Masson's Trichrome in control or C3aR1-KpKO
337 male mice (scale bar = 100 mm).
338 F) Lipid droplet area quantified on liver sections of control or C3aR1-KpKO male mice,
339 excluding vessel lumens (n = 8-9).
340 G) Collagen area quantified on whole liver section of control or C3aR1-KpKO male mice (n=
341 8-9).
342 H) Relative gene expression in male control or C3aR1-KpKO mice after 30 weeks GAN diet
343 (n = 5-6).

344 Unpaired two-tailed Student's *t* test: **, $p < 0.01$.

345

346 **Supplementary figures.**

347 S1) Single cell RNA sequencing analysis of *C3ar1* expression in mouse liver tissue (see
348 text).

349 S2) Percent lean and fat mass of flox/flox control mice after 20 weeks of GAN or RD (n = 6-7
350 per group).

351 S3) Absolute lean and fat mass of flox/flox control mice after 20 weeks of GAN or RD (n = 6-
352 7 per group).

353 S4) Relative gene expression in control female mice after 33 weeks on RD (n = 4-6 per
354 group).

355 S5) Insulin tolerance test in control or C3aR1-MφKO male mice with 14h fast after 29 weeks
356 GAN diet (n = 6-9 per group).

357 S6) HOMA-IR measurement of insulin resistance in control or C3aR1-MφKO mice with 6h
358 fast after 27 weeks GAN diet (n = 6-9 per male group, n = 9-13 per female group).

359 S7) Serum alanine aminotransferase levels in control or C3aR1-MφKO male mice after 30
360 weeks GAN diet (n = 4 per group).

361 S8) Relative gene expression in control or C3aR1-MφKO female mice after 30 weeks of
362 either GAN (n = 13-14 per group) or RD (n = 5-6 per group).

363 S9) Relative *C3ar1* expression in control or C3aR1-KpKO female mice after 30 weeks RD (n
364 = 2-3 per group).

365 Unpaired two-tailed Student's *t* test: **, $p < 0.01$; ***, $p < 0.001$.

366

Supplementary Table S1.

***Mus musculus* gene name**	**Forward qPCR primer**	**Reverse qPCR primer**
Acc2	GCCTCCACTCACATTGGTTT	ATTGAAGAAAGCTGGGCTGA
Acta2	GGCTCTGGGCTCTGTAAGG	CTCTTGCTCTGGGCTTCATC
Adgre1	TGCATCTAGCAATGGACAGC	GCCTTCTGGATCCATTTGAA
C3ar1	TGACAGGTCAGCTCCTTCCT	CATTAGGAGGCTTTCCACCA
Ccr2	ATCCACGGCATACTATCAACATC	CAAGGCTCACCATCATCGTAG
Cd163	TCCACACGTCCAGAACAGTC	CCTTGGAAACAGAGACAGGC
Cfd	CGTACCATGACGGGGTAGTC	ATCCGGTAGGATGACACTCG
Col1a1	GTGCTCCTGGTATTGCTGGT	GGCTCCTCGTTTTCCTTCTT
Col1a2	GCCACCATTGATAGTCTCTCC	CACCCCAGCGAAGAACTCATA
Col3a1	GGGTTTCCCTGGTCCTAAAG	CCTGGTTTCCCATTTTCTCC
Fasn	TTGCTGGCACTACAGAATGC	AACAGCCTCAGAGCGACAAT
Fgf21	CTGCTGGGGGTCTACCAAG	CTGCGCCTACCACTGTTCC
Hnf1a	GACCTGACCGAGTTGCCTAAT	CCGGCTCTTTCAGAATGGGT
Il1b	CTGGTGTGTGACGTTCCCATTA	CCGACAGCACGAGGCTTT
Il6	ACAACCACGGCCTTCCCTACTT	CACGATTTCCCAGAGAACATGTG
Pepck1	TCATCATCACCCAAGAGCAG	CACATAGGGCGAGTCTGTCA
Rps18	CATGCAGAACCCACGACAGTA	CCTCACGCAGCTTGTTGTCTA
Scd1	CGCCCAAGCTGGAGTACGTC	CGCCCAAGCTGGAGTACGTC
Srebp1c	CTGGCAGTTCCATTGACAAG	ACTGAAGCTGGTGACTGCTG
Tgfb1	TGCGCTTGCAGAGATTAAAA	AGCCCTGTATTCCGTCTCCT
Tlr4	TGTCATCAGGGACTTTGCTG	GGACTCTGATCATGGCACTG
Tnfa	ACGGCATGGATCTCAAAGAC	AGATAGCAAATCGGCTGACG
Trem2	CTACCAGTGTCAGAGTCTCCGA	CCTCGAAACTCGATGACTCCTC

References

1 Ge, X., Zheng, L., Wang, M., Du, Y. & Jiang, J. Prevalence trends in non-alcoholic fatty liver disease at the global, regional and national levels, 1990-2017: a population-based observational study. *BMJ Open* **10**, e036663 (2020). https://doi.org:10.1136/bmjopen-2019-036663

2 Younossi, Z. *et al.* Global burden of NAFLD and NASH: trends, predictions, risk factors and prevention. *Nat Rev Gastroenterol Hepatol* **15**, 11-20 (2018). https://doi.org:10.1038/nrgastro.2017.109

3 Ferguson, D. & Finck, B. N. Emerging therapeutic approaches for the treatment of NAFLD and type 2 diabetes mellitus. *Nat Rev Endocrinol* **17**, 484-495 (2021). https://doi.org:10.1038/s41574-021-00507-z

4 Friedman, S. L., Neuschwander-Tetri, B. A., Rinella, M. & Sanyal, A. J. Mechanisms of NAFLD development and therapeutic strategies. *Nat Med* **24**, 908-922 (2018). https://doi.org:10.1038/s41591-018-0104-9

5 Stefan, N., Haring, H. U. & Cusi, K. Non-alcoholic fatty liver disease: causes, diagnosis, cardiometabolic consequences, and treatment strategies. *Lancet Diabetes Endocrinol* **7**, 313-324 (2019). https://doi.org:10.1016/S2213-8587(18)30154-2

6 Kim, H. *et al.* Metabolic Spectrum of Liver Failure in Type 2 Diabetes and Obesity: From NAFLD to NASH to HCC. *Int J Mol Sci* **22** (2021). https://doi.org:10.3390/ijms22094495

7 Duell, P. B. *et al.* Nonalcoholic Fatty Liver Disease and Cardiovascular Risk: A Scientific Statement From the American Heart Association. *Arterioscler Thromb Vasc Biol* **42**, e168-e185 (2022). https://doi.org:10.1161/ATV.0000000000000153

8 Kasper, P. *et al.* NAFLD and cardiovascular diseases: a clinical review. *Clin Res Cardiol* **110**, 921-937 (2021). https://doi.org:10.1007/s00392-020-01709-7

9 Barreby, E., Chen, P. & Aouadi, M. Macrophage functional diversity in NAFLD - more than inflammation. *Nat Rev Endocrinol* **18**, 461-472 (2022). https://doi.org:10.1038/s41574-022-00675-6

10 Cai, J., Zhang, X. J. & Li, H. The Role of Innate Immune Cells in Nonalcoholic Steatohepatitis. *Hepatology* **70**, 1026-1037 (2019). https://doi.org:10.1002/hep.30506

11 Guilliams, M. & Scott, C. L. Liver macrophages in health and disease. *Immunity* **55**, 1515-1529 (2022). https://doi.org:10.1016/j.immuni.2022.08.002

12 Park, S. J., Garcia Diaz, J., Um, E. & Hahn, Y. S. Major roles of kupffer cells and macrophages in NAFLD development. *Front Endocrinol (Lausanne)* **14**, 1150118 (2023). https://doi.org:10.3389/fendo.2023.1150118

13 Sakai, M. *et al.* Liver-Derived Signals Sequentially Reprogram Myeloid Enhancers to Initiate and Maintain Kupffer Cell Identity. *Immunity* **51**, 655-670 e658 (2019). https://doi.org:10.1016/j.immuni.2019.09.002

14 Krenkel, O. *et al.* Myeloid cells in liver and bone marrow acquire a functionally distinct inflammatory phenotype during obesity-related steatohepatitis. *Gut* **69**, 551-563 (2020). https://doi.org:10.1136/gutjnl-2019-318382

15 Guilliams, M. *et al.* Spatial proteogenomics reveals distinct and evolutionarily conserved hepatic macrophage niches. *Cell* **185**, 379-396 e338 (2022). https://doi.org:10.1016/j.cell.2021.12.018

16 Govaere, O. *et al.* Transcriptomic profiling across the nonalcoholic fatty liver disease spectrum reveals gene signatures for steatohepatitis and fibrosis. *Sci Transl Med* **12** (2020). https://doi.org:10.1126/scitranslmed.aba4448

17 Merle, N. S., Church, S. E., Fremeaux-Bacchi, V. & Roumenina, L. T. Complement System Part I - Molecular Mechanisms of Activation and Regulation. *Front Immunol* **6**, 262 (2015). https://doi.org:10.3389/fimmu.2015.00262

18 Kolev, M. & Kemper, C. Keeping It All Going-Complement Meets Metabolism. *Front Immunol* **8**, 1 (2017). https://doi.org:10.3389/fimmu.2017.00001

19 Zhao, J. *et al.* Association of complement components with the risk and severity of NAFLD: A systematic review and meta-analysis. *Front Immunol* **13**, 1054159 (2022). https://doi.org:10.3389/fimmu.2022.1054159

20 Segers, F. M. *et al.* Complement alternative pathway activation in human nonalcoholic steatohepatitis. *PLoS One* **9**, e110053 (2014). https://doi.org:10.1371/journal.pone.0110053

21 Markiewski, M. M. & Lambris, J. D. The role of complement in inflammatory diseases from behind the scenes into the spotlight. *Am J Pathol* **171**, 715-727 (2007). https://doi.org:10.2353/ajpath.2007.070166

22 Yadav, M. K. *et al.* Molecular basis of anaphylatoxin binding, activation, and signaling bias at complement receptors. *Cell* **186**, 4956-4973 e4921 (2023). https://doi.org:10.1016/j.cell.2023.09.020

23 Flier, J. S., Cook, K. S., Usher, P. & Spiegelman, B. M. Severely impaired adipsin expression in genetic and acquired obesity. *Science* **237**, 405-408 (1987). https://doi.org:10.1126/science.3299706

24 Xu, Y. *et al.* Complement activation in factor D-deficient mice. *Proc Natl Acad Sci U S A* **98**, 14577-14582 (2001). https://doi.org:10.1073/pnas.261428398

25 Lim, J. *et al.* C5aR and C3aR antagonists each inhibit diet-induced obesity, metabolic dysfunction, and adipocyte and macrophage signaling. *FASEB J* **27**, 822-831 (2013). https://doi.org:10.1096/fj.12-220582

26 Polyzos, S. A., Kountouras, J. & Mantzoros, C. S. Adipokines in nonalcoholic fatty liver disease. *Metabolism* **65**, 1062-1079 (2016). https://doi.org:10.1016/j.metabol.2015.11.006

27 Han, J. & Zhang, X. Complement Component C3: A Novel Biomarker Participating in the Pathogenesis of Non-alcoholic Fatty Liver Disease. *Front Med (Lausanne)* **8**, 653293 (2021). https://doi.org:10.3389/fmed.2021.653293

28 Lo, J. C. *et al.* Adipsin is an adipokine that improves beta cell function in diabetes. *Cell* **158**, 41-53 (2014). https://doi.org:10.1016/j.cell.2014.06.005

29 Gomez-Banoy, N. *et al.* Adipsin preserves beta cells in diabetic mice and associates with protection from type 2 diabetes in humans. *Nat Med* **25**, 1739-1747 (2019). https://doi.org:10.1038/s41591-019-0610-4

30 Mamane, Y. *et al.* The C3a anaphylatoxin receptor is a key mediator of insulin resistance and functions by modulating adipose tissue macrophage infiltration and activation. *Diabetes* **58**, 2006-2017 (2009). https://doi.org:10.2337/db09-0323

31 Han, J. *et al.* Bone marrow-derived macrophage contributes to fibrosing steatohepatitis through activating hepatic stellate cells. *J Pathol* **248**, 488-500 (2019). https://doi.org:10.1002/path.5275

32 Boland, M. L. *et al.* Towards a standard diet-induced and biopsy-confirmed mouse model of non-alcoholic steatohepatitis: Impact of dietary fat source. *World J Gastroenterol* **25**, 4904-4920 (2019). https://doi.org:10.3748/wjg.v25.i33.4904

33 Hansen, H. H. *et al.* Human translatability of the GAN diet-induced obese mouse model of non-alcoholic steatohepatitis. *BMC Gastroenterol* **20**, 210 (2020). https://doi.org:10.1186/s12876-020-01356-2

34 Vacca, M. *et al.* An unbiased ranking of murine dietary models based on their proximity to human metabolic dysfunction-associated steatotic liver disease (MASLD). *Nat Metab* (2024). https://doi.org:10.1038/s42255-024-01043-6

35 Uhlen, M. *et al.* Proteomics. Tissue-based map of the human proteome. *Science* **347**, 1260419 (2015). https://doi.org:10.1126/science.1260419

36 MacParland, S. A. *et al.* Single cell RNA sequencing of human liver reveals distinct intrahepatic macrophage populations. *Nat Commun* **9**, 4383 (2018). https://doi.org:10.1038/s41467-018-06318-7

37 Tabula Muris, C. *et al.* Single-cell transcriptomics of 20 mouse organs creates a Tabula Muris. *Nature* **562**, 367-372 (2018). https://doi.org:10.1038/s41586-018-0590-4

38 Suppli, M. P. *et al.* Hepatic transcriptome signatures in patients with varying degrees of nonalcoholic fatty liver disease compared with healthy normal-weight individuals. *Am J Physiol Gastrointest Liver Physiol* **316**, G462-G472 (2019). https://doi.org:10.1152/ajpgi.00358.2018

39 Ma, L. *et al.* Adipsin and Adipocyte-derived C3aR1 Regulate Thermogenic Fat in a Sex-dependent Fashion. *JCI Insight* (2024). https://doi.org:10.1172/jci.insight.178925

40 Kong, L. R. *et al.* Loss of C3a and C5a receptors promotes adipocyte browning and attenuates diet-induced obesity via activating inosine/A2aR pathway. *Cell Rep* **42**, 112078 (2023). https://doi.org:10.1016/j.celrep.2023.112078

41 Li, X. *et al.* A new NASH model in aged mice with rapid progression of steatohepatitis and fibrosis. *PLoS One* **18**, e0286257 (2023). https://doi.org:10.1371/journal.pone.0286257

42 Tsuchida, T. *et al.* A simple diet- and chemical-induced murine NASH model with rapid progression of steatohepatitis, fibrosis and liver cancer. *J Hepatol* **69**, 385-395 (2018). https://doi.org:10.1016/j.jhep.2018.03.011

43 Cumpelik, A. *et al.* Dynamic regulation of B cell complement signaling is integral to germinal center responses. *Nat Immunol* **22**, 757-768 (2021). https://doi.org:10.1038/s41590-021-00926-0

44 Zhang, X., Goncalves, R. & Mosser, D. M. The isolation and characterization of murine macrophages. *Curr Protoc Immunol* **Chapter 14**, 14 11 11-14 11 14 (2008). https://doi.org:10.1002/0471142735.im1401s83

Figure 1.

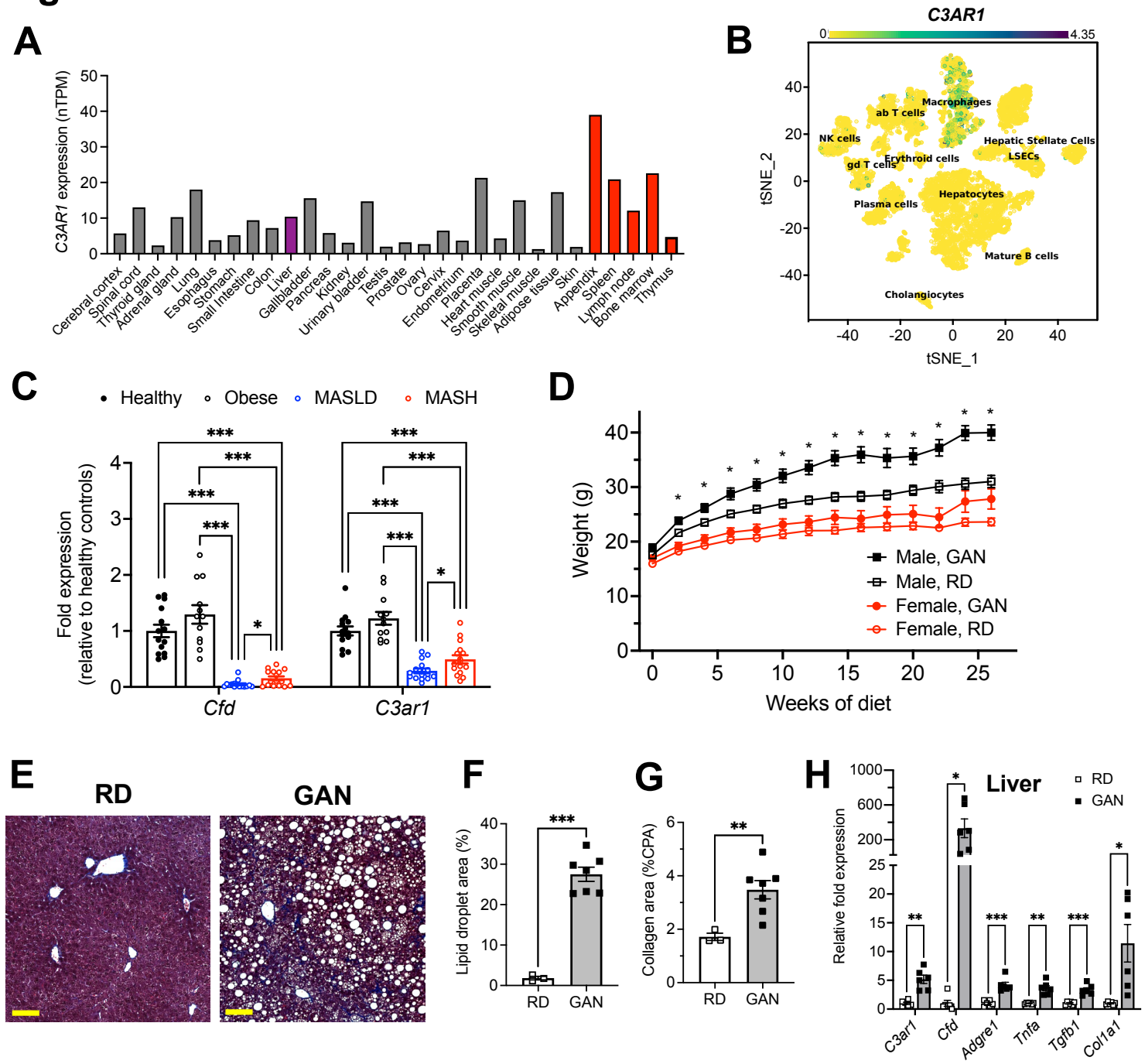

Figure 1. C3AR1 is found in macrophages, is modulated by MASLD/MASH in humans, and is induced by a murine dietary model of MASH.

A) Relative *C3AR1* human tissue expression level by tissue, derived from deep sequencing of the mRNA combined dataset (HPA and GTEx) in the Human Protein Atlas, shown as normalized transcripts per million (nTPM). Liver is highlighted in purple and immunologic tissues are highlighted in red.

B) Single-cell RNA sequencing distribution of *C3AR1* expression in human liver (tSNE, t-distributed Stochastic Neighbor Embedding).

C) Analysis of *CFD* and *C3AR1* expression from liver biopsy samples in patients with MASH, MASLD, obesity without MASLD, and age-matched healthy controls (n = 12-16 per group, Welch *t* test with Holm-Šídák correction for multiple comparisons).

D) Weight curve in male and female flox/flox control mice placed on GAN high-fat diet compared to regular diet (RD) controls (males, n = 7; females, n = 6).

E) Representative liver section staining by Masson's Trichrome in male control mice on RD or GAN diet for 28 weeks (scale bar = 100 μm).

F) Lipid droplet area quantification in liver sections from male control mice, excluding vessel lumens (RD, n = 3; GAN, n = 7).

G) Collagen area quantification in liver sections of male control mice (RD, n = 3; GAN, n = 7).

H) Gene expression of key macrophage or fibrosis genes in male control mice on GAN or RD (n = 6 per group).

Unpaired two-tailed Student's *t* test (Except 1C as above). Annotations: *, $p < 0.05$; **, $p < 0.01$; ***, $p < 0.001$.

Figure 2.

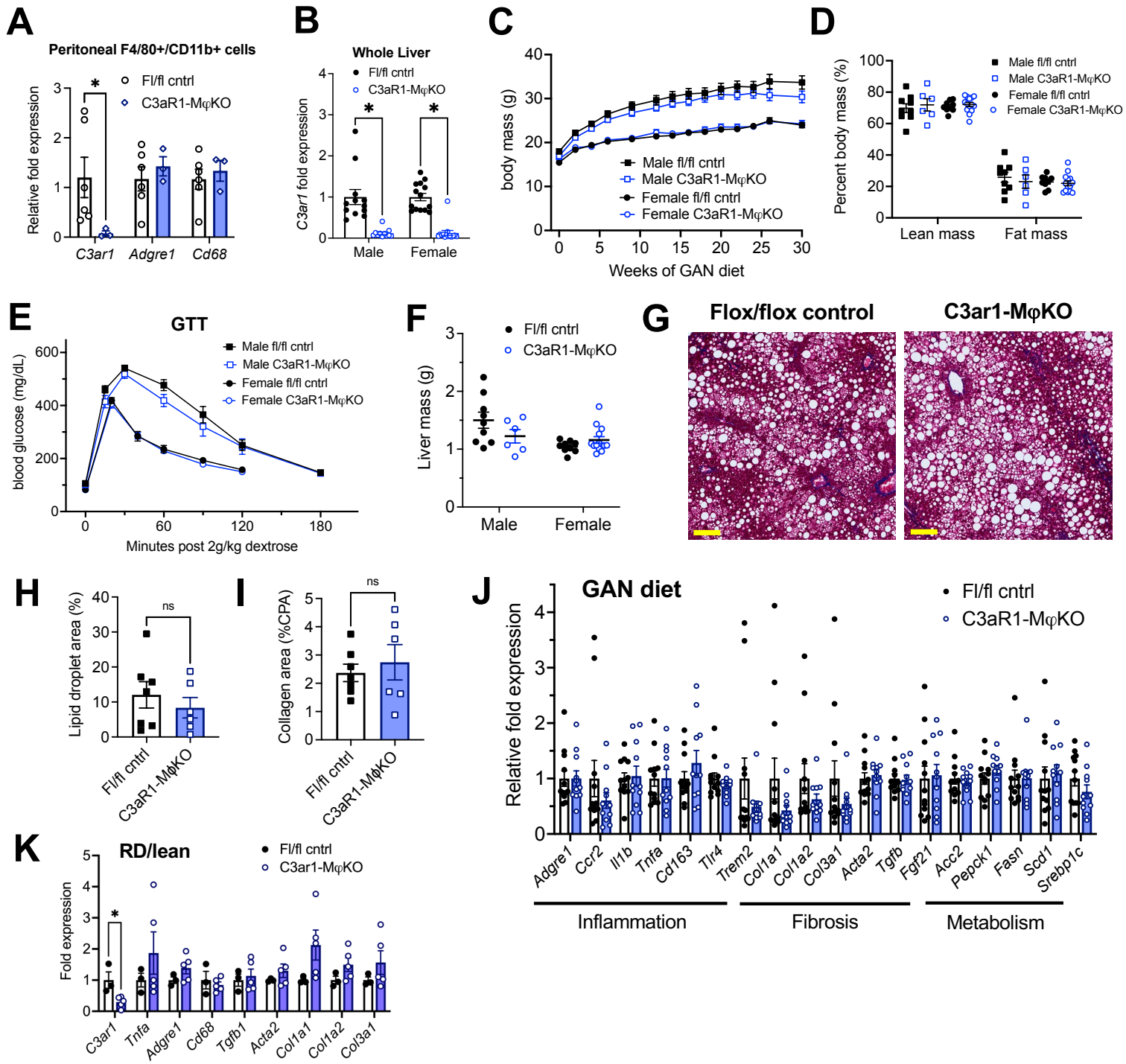

Figure 2. C3aR1 deletion in all macrophages does not affect weight gain, glucose homeostasis, liver steatosis or fibrosis.

A) Expression of *C3ar1* in isolated peritoneal F4/80+/CD68+ cells from control mice (n = 6) or C3aR1-MφKO male mice (n = 3).
B) Expression of *C3ar1* in whole liver from control or C3aR1-MφKO mice (n = 11-12 per male group, n = 13-14 per female group).
C) Body mass curve of control or C3aR1-MφKO mice on GAN high-fat diet starting at 5 weeks of age (n = 11-12 per male group, n = 14 per female group).
D) Body composition analysis by EchoMRI in control or C3aR1-MφKO mice after 30 weeks GAN diet (n = 6-9 per male group, n = 9-13 per female group).
E) Glucose tolerance test in control or C3aR1-MφKO mice with 14h fast after 28 weeks GAN diet (n = 6-9 per male group, n = 9-14 per female group).
F) Liver mass in control or C3ar1-MφKO male mice at time of euthanasia after 30 weeks GAN diet (n = 6-9 per male group, n = 9-14 per female group).
G) Representative liver section staining by Masson's Trichrome in male control or C3ar1-MφKO mice (scale bar = 100 μm).
H) Lipid droplet area in liver sections from male control or C3ar1-MφKO mice, excluding vessel lumens (n = 6-7 per group).
I) Collagen area in liver sections from male control or C3ar1-MφKO mice (n = 6-7 per group).
J,K) Relative mRNA expression of key markers for inflammation, fibrosis, and liver metabolism in liver from male control or C3ar1-MφKO mice after 30 weeks of either GAN (J) diet (n = 11-12 per group) or regular (K) diet (n = 3-5 per group).
Unpaired two-tailed Student's *t* test: Student's *t* test: *, $p < 0.05$.

Figure 3.

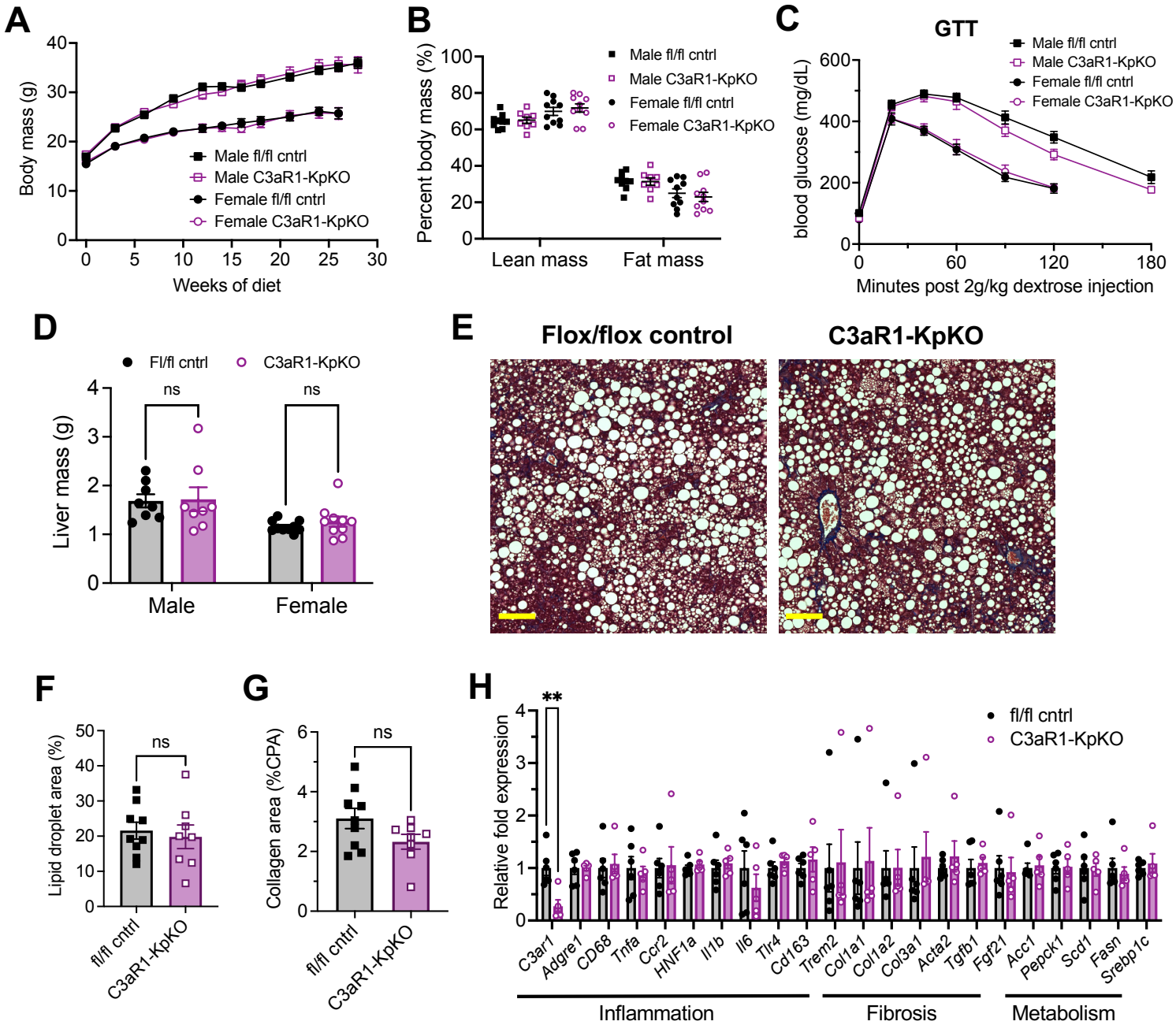

Figure 3. C3aR1 deletion in Kupffer cells does not affect weight gain, glucose homeostasis, liver steatosis or fibrosis.

A) Body mass on GAN diet in flox/flox control or C3aR1-KpKO mice beginning at 5 weeks of age (n = 8-10 per group).
B) Body composition analysis by EchoMRI in control or C3aR1-KpKO mice after 28 weeks GAN diet (n = 8-10).
C) Glucose tolerance test in control or C3aR1-KpKO mice with 14h fast after 26 weeks GAN diet (n = 8-10).
D) Liver mass in control or C3aR1-KpKO male mice at time of euthanasia after 28 weeks GAN diet (n = 8-10).
E) Representative liver section staining by Masson's Trichrome in control or C3aR1-KpKO male mice (scale bar = 100 μm).
F) Lipid droplet area quantified on liver sections of control or C3aR1-KpKO male mice, excluding vessel lumens (n = 8-9).
G) Collagen area quantified on whole liver section of control or C3aR1-KpKO male mice (n= 8-9).
H) Relative gene expression in control or C3aR1-KpKO male mice after 30 weeks GAN diet (n = 5-6).

Unpaired two-tailed Student's *t* test: **, $p < 0.01$.

Supplementary Figures.

S1

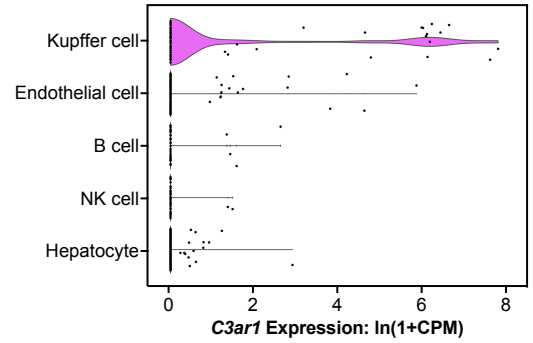

S2

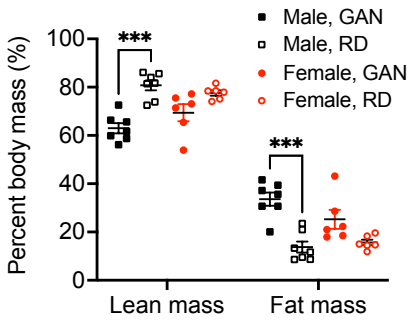

S3

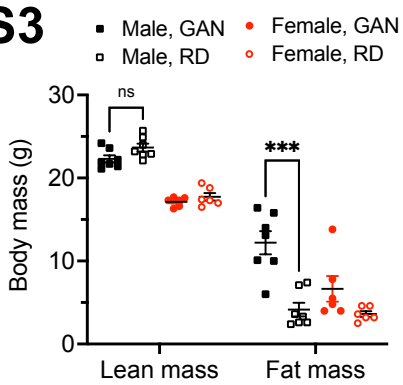

S4

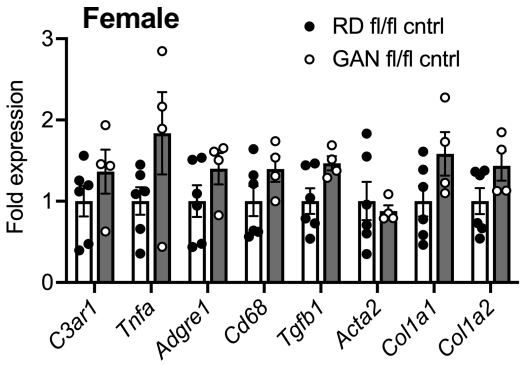

S5

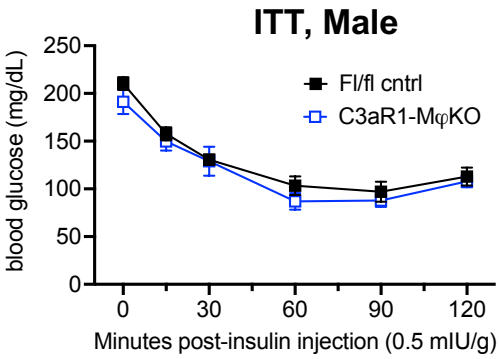

S6

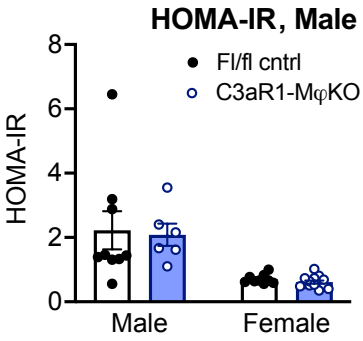

S7

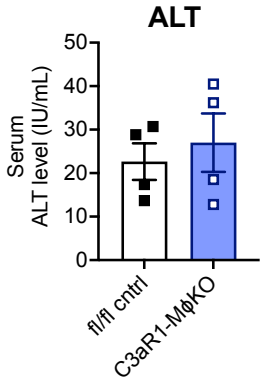

S8

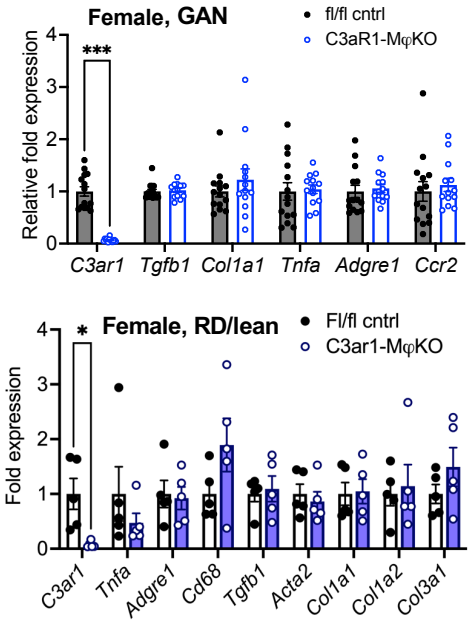

S9

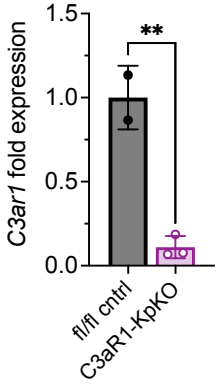

Supplementary figures.

S1) Single cell RNA sequencing analysis of *C3ar1* expression in mouse liver tissue (see text).
S2) Percent lean and fat mass of flox/flox control mice after 20 weeks of GAN or RD (n = 6-7 per group).
S3) Absolute lean and fat mass of flox/flox control mice after 20 weeks of GAN or RD (n = 6-7 per group).
S4) Relative gene expression in control female mice after 30 weeks on RD (n = 4-6 per group).
S5) Insulin tolerance test in control or C3aR1-MφKO male mice with 14h fast after 29 weeks GAN diet (n = 6-9 per group).
S6) HOMA-IR measurement of insulin resistance in control or C3aR1-MφKO mice with 6h fast after 27 weeks GAN diet (n = 6-9 per male group, n = 9-13 per female group).
S7) Serum alanine aminotransferase levels in control or C3aR1-MφKO male mice after 30 weeks GAN diet (n = 4 per group).
S8) Relative gene expression in control or C3aR1-MφKO female mice after 30 weeks of either GAN (n = 13-14 per group) or RD (n = 5-6 per group).
S9) Relative *C3ar1* expression in control or C3aR1-KpKO female mice after 30 weeks RD (n = 2-3 per group).
Unpaired two-tailed Student's *t* test: **, $p < 0.01$; ***, $p < 0.001$.